THE JOURNAL OF PHYSICAL CHEMISTRY B

Article

pubs.acs.org/JPCB

The Structural Role of Mg^{2+} Ions in a Class I RNA Polymerase Ribozyme: A Molecular Simulation Study

Jacopo Sgrignani and Alessandra Magistrato*

CNR-IOM-Democritos National Simulation Center C/o International Studies for Advanced Studies (SISSA/ISAS), Via Bonomea 265, 34165, Trieste, Italy

Supporting Information

ABSTRACT: According to the RNA world hypothesis, self-replicating ribozymes, storing the genetic information and being able to perform catalysis, were the constituents of the first living organisms. In particular, RNA polymerase ribozymes, similar to current proteinaceous enzymatic polymerases, may have been able to promote the synthesis of RNA strands in a primitive world. Polymerase catalysis is usually assisted by Mg^{2+} ions, but it is not always trivial to find out experimentally the number of Mg^{2+} ions placed in the active site as well as the identity and the number of their coordination ligands. Here, we addressed this issue in an artificial class I ligase ribozyme. On the basis of a recently solved crystal structure, we constructed computational models of reactant and product states of this ribozyme, considering monometallic and bimetallic species. Our models were relaxed by force field based molecular dynamics (MD) simulations and mixed quantum-classical (QM/MM) MD. The structural and dynamical properties of these models were consistent with experimental data and were validated by a comparison with the catalytic sites of proteinaceous DNA and RNA polymerases. Consistently with enzymatic polymerases, our results suggest that class I RNA ligases most probably contain two magnesium ions in the active site and they may, therefore, catalyze the junction of two RNA strands via "a two Mg^{2+} ions" mechanism.

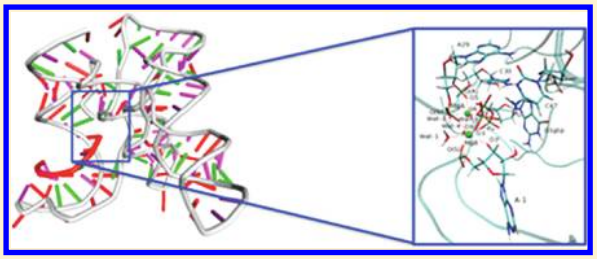

1. INTRODUCTION

RNA enzymes (usually termed ribozymes) have catalytic centers entirely composed by RNA, and they do not require proteins for catalysis. Their discovery, in the 1980s, resulted in the "RNA world hypothesis", according to which self-replicating RNA molecules may have been the constituents of the first living organisms, being simultaneously genome and catalysts.[1,2] Although most enzymes are proteins, the discovery of naturally occurring ribozymes that catalyze phosphodiester bond isomerization, hydrolysis, and peptide bond formation[3,4] has confirmed the reliability of the "RNA world hypothesis" as well as the central role of RNA also in modern living forms. Despite the research efforts in this field, no naturally occurring polymerase ribozyme has been discovered to date. Therefore, many attempts have been devoted to generate this kind of ribozymes via *in vitro* evolution methods.[5−7] Usually the evolution of this kind of ribozymes goes through the formation of a ligase, and only after this is evolved to a polymerase. Both polymerases and ligases catalyze the reaction between the 3′-hydroxyl group of an oligonucleotide and the 5′-Pα of a nucleotide triphosphate (NTP) (Figure 1A). However, while ligases simply join two RNA oligonucleotides, polymerases, instead, catalyze the addiction of multiple NTPs consecutively and in a sequence dependent manner (Figure 1B and C). The efficiency of polymerase ribozymes is usually low, as they can undergo a limited number of catalytic cycles.[6] In fact, a ribozyme capable of catalyzing RNA synthesis up to 95 nucleotides has been created only recently.[8]

Understanding the structural and catalytic properties of class I RNA ligase ribozymes is, therefore, of fundamental importance to direct the design of an RNA-catalyzed RNA polymerization with improved catalytic performances.

Class I RNA ligases are particularly interesting, since they are very fast ribozymes (with a catalytic rate of up to 360 per minute)[9] operative at different pHs and magnesium concentrations.[10−14] Moreover, at variance with the other classes, class I ribozymes are specific for the formation of a phosphodiester bond between the 3′-hydroxyl group of an oligonucleotide substrate and its own 5′-α-phosphate. The presence of metal ions is frequently related with the catalytic activity of most ribozymes,[15−17] as well as to that of the corresponding proteinaceous enzymes.[4,18]

In particular, Mg^{2+} ions play a key role as (i) they usually screen the negative charge of the phosphate backbone allowing the ribozyme to fold into the catalytic competent form; (ii) they coordinate the functional groups of the ribozymes and of the substrates, placing them in the correct position for the catalytic reaction; (iii) they often facilitate acid base catalysis, affecting the pK_a of the nucleophiles involved in the reaction; (iv) they stabilize the transition states of the catalytic cycle.[18−21] Therefore, detailed structural information about the metal content, the identification of the binding sites, and

Received: July 8, 2011
Revised: January 9, 2012
Published: January 23, 2012

dx.doi.org/10.1021/jp206475d | J. Phys. Chem. B 2012, 116, 2259−2268

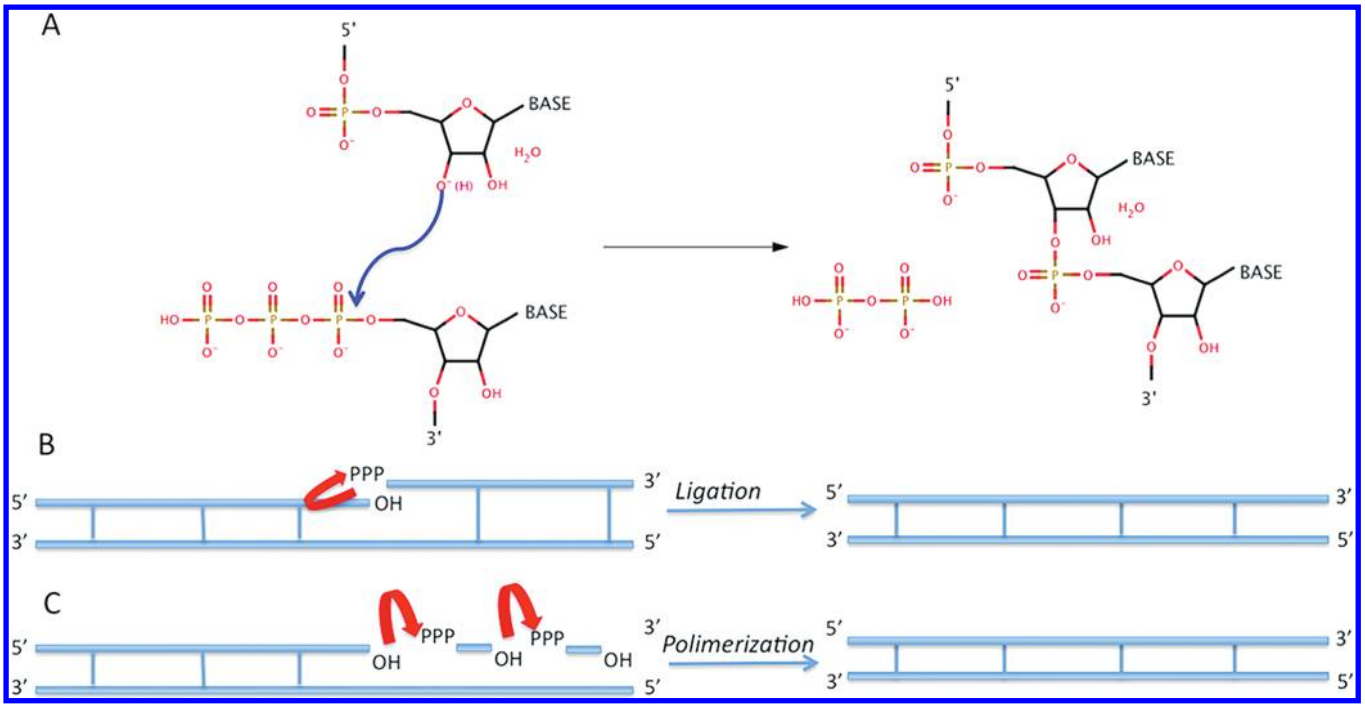

Figure 1. (A) General scheme of an RNA polymerase reaction. In a ligase, the 3′ end of the nucleotide is joined to an RNA oligonucleotide. Scheme of a ligase and polymerase catalytic reaction in parts B and C, respectively.

the coordination ligands appears to be of crucial importance to shed light on the catalytic mechanism of this fascinating class of enzymes.

Here, we focused on a class I RNA polymerase ribozyme (Figure 2), particularly tolerant to low magnesium concentration, whose structure was recently solved.[6] In particular, this

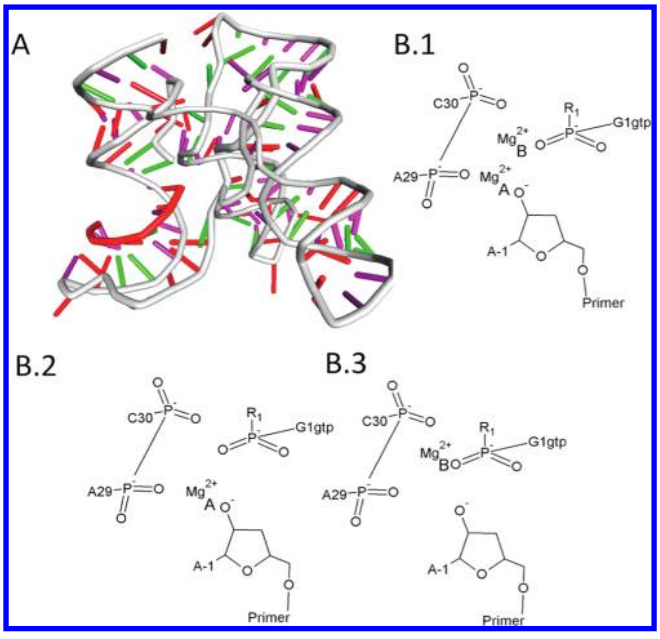

Figure 2. (A) Cartoon of the X-ray structure of the class I RNA polymerase ribozyme (pdb code 3IVK). The ribozyme and the substrate backbone atoms are colored in gray and red, respectively. Different models of the catalytic site considered in this work AdMgAB (B.1), AdMgA (B.2), and AdMgB (B.3).

ribozyme represents a challenging system to study computationally, since the crystal structure solved by Shechner et al.[6] is that of an autoligation product and no metal ion was detected inside the hypothetical catalytic site. Unfortunately, Mg^{2+} is spectroscopically silent so when the ion is not detected crystallographically, it is challenging to obtain experimental information about its exact location and its role in the catalytic site. In this case, nucleotide analog interfering mapping (NAIM) experiments suggested that the catalytic site is formed by G1, A29, C30, and C47 and that at least one Mg^{2+} ion is coordinated at this site,[6,22] in analogy with other natural self-splicing[23,24] and with another ligase[5] ribozymes. Over the years, different experimental and theoretical approaches have been applied to the study of metal−RNA interactions.[17] Nowadays, molecular simulations represent a reliable alternative to address these issues, complementing experimental findings, when they provide only indirect information on the Mg^{2+} binding sites.[25] In fact, many theoretical studies can provide an atomistic picture of metal containing biological systems[26−31] or clarify their enzymatic mechanisms.[32−35] Since the binding of metal ions comes along with charge transfer and polarization effects, an explicit treatment of the electronic degrees of freedom, such as in QM/MM calculations, is most often mandatory.[27,36−39]

Therefore, we applied a variety of computational approaches, spanning from force field (FF) based molecular dynamics (MD) simulations to hybrid quantum-classical (QM/MM) MD, to provide a structural characterization for the binding of Mg^{2+} ions inside the catalytic pocket.

The reliability of our structural models was validated by a comparison with experimental findings.[5,6,40] In addition, the generality of our results was confirmed by a comparison with the structural properties of proteinaceous RNA and DNA polymerases and other naturally occurring ribozymes.[41−49] Consistently with experimental suggestions[6] and with Steitz's hypothesis,[50] we suggest that two Mg^{2+} ions are most likely

dx.doi.org/10.1021/jp206475d | J. Phys. Chem. B 2012, 116, 2259−2268

necessary for the binding of the substrate in a favorable position to have the ligation of two RNA tracts.

2. COMPUTATIONAL METHODS

2.1. Model Systems. Starting from the crystal structure of the class I RNA polymerase (pdb code: 3IVK, Figure 2A),[6] which represents an autoligation product, we constructed three models of the product state. In all models, the 16 crystallographic Mg^{2+} ions were conserved. Moreover, to ensure electroneutrality and to localize Mg^{2+} ions in the vicinity of the putative catalytic site, we added Mg^{2+} and Na^{+} ions in different number in the most negative regions of the electrostatic potential.

Applying this procedure, we obtained three different models P1 (16 Mg^{2+}, 95 Na^{+}), P2 (46 Mg^{2+}, 34 Na^{+}), and P3 (61 Mg^{2+}, 5 Na^{+}). These models correspond to a Mg^{2} concentration of 38, 109, and 144 mM and to a Na^{+} concentration of 225, 88, and 11 mM, respectively.

P2 resulted to be the model hosting a Mg^{2+} in the active site and with the minimal amount of added Mg^{2+}. (We remark that even adding a very large amount of Mg^{2+} it is not possible to detect two Mg^{2+} ions in the catalytic site.) Moreover, this model reproduces the ratio between the concentration of ribozyme and that of Mg^{2+} used experimentally.[6] In addition, since Na^{+} is known to have an inhibitory effect at low Mg^{2+} concentration, we avoided using a model with a very large concentration of Na^{+}, which may compete with Mg^{2+} to bind in the catalytic site. After having verified its structural stability (vide infra), the equilibrated structure of P2 was used as a starting structure to construct models of the ribozyme/substrate adducts. In these models, the bond between the O3′@A-1 and Pα@G1 was removed and a triphosphate moiety was added to G1 (from here on named $G1_{gtp}$). The three adduct models differed in the number and in the location of putative catalytic Mg^{2+} ion(s) (Figure 2B−D): in model AdMgA, a Mg^{2+} was placed between the A29 and C30 phosphate groups (termed A binding site and the ion placed inside was termed MgA). In model AdMgAB, in addition to MgA, a second Mg^{2+} was placed near the pyrophosphate moiety (PPi) of a guanosine triphosphate ($G1_{gtp}$), at a distance of 4 Å from MgA (MgB, in the B site). Finally, in AdMgB, a Mg^{2+} was placed in the B site only. The starting geometries of the adducts were manually built inserting the PPi moiety in the equilibrated structure of P2, obtained from previous MD runs. Due to the introduction of the PPi moiety, two additional Na^{+} ions were added to AdMgA and AdMgB to ensure electroneutrality. These were placed according to the electrostatic potential. Since measurements of the catalytic activity[22] and the crystallization process[6] were carried out at pH 6.0, we protonated $G1_{gtp}$ on Oγ, as proposed in ref 6. In addition, we remark that the O3′@A-1 was left deprotonated. This was done to simulate a preactivated nucleophile, which may allow a more realistic hypotheses on the reaction mechanism to be formulated.

In addition, the adducts, which resulted to be stable after the classical MD and QM/MM MD runs, were simulated also considering the C47U mutation. This was shown to decrease the catalytic activity by a factor larger than 10^4. The models of the mutants will be labeled as those of the adducts followed by C47U (i.e., AdMgAB-C47U).

2.2. Force Field Based MD simulations. The PARM99[51] version of the AMBER FF, along with the corrections recently developed for nucleic acids,[52] was used for the RNA. For the sodium and magnesium counterions, we used the parametrization of Åqvist.[53] The TIP3P water model was employed.[54] The FF parameters to simulate the γ protonated guanosine triphosphate (GTP) were taken from ref 55, while the atomic charges of GTP were calculated using the RESP methodology (i.e., fitting an electrostatic potential calculated at the HF/6-31G* level of theory with the Gaussian 03 program).[56] The ribozyme was solvated using a box of waters of at least 12 Å from the most solvent exposed residues. The resulting models were composed by ∼62,600 atoms.

The topologies were prepared using the *leap* module of AMBER11.[57] The systems were simulated in an isothermal−isobaric ensemble (NPT) with NAMD 2.7,[58] using Langevin dynamics (298.5 K) and a Langevin piston (1 atm). The long-range Columbic electrostatic interactions were evaluated using the particle mesh Ewald summation method (PME), while the Lennard−Jones potential was smoothly cut off between 10 and 12 Å. In all simulations, a time step of 1.5 fs was used.

We initially verified that the structural integrity of the ribozyme was independent from the ionic concentration (Figure S1 in the Supporting Information) by performing a set of simulations of 30 ns with the AMBER point charges for Mg^{2+}. Then, we further refined the P2 model by performing an additional 20 ns of MD using the dummy cation approach of Oelschlaeger et al. for the Mg^{2+} ions.[59,60] In this parametrization, Mg^{2+} is surrounded by six dummy atoms parametrized to reproduce both the geometrical and energetic features of the magnesium ion. We have adopted this computational protocol as no Mg^{2+} was detected crystallographically in the active site. Therefore, we used initially the point charge model because we wanted to see if any Mg^{2+} could accommodate in the vicinity of the ribozyme, occupying a position slightly different from that assigned on the basis of the elecrostatic potential. Then, once the position of the Mg^{2+} was established and equilibrated, we employed the dummy cation approach, to describe more realistically the coordination geometry of the metal binding site.

2.3. QM/MM MD Calculations. To further refine the geometry of the metal coordination site(s) obtained from classical MD simulations, we also performed 6 ps Born−Oppenheimer QM/MM MD[61] using the CP2K program.[62] In these simulations, we treated at the QM level only the coordination spheres of the Mg^{2+} ions. 62 atoms were included in the QM part for AdMgAB, and 42 atoms, for AdMgB (a complete list of the atoms in the QM part is available in Table S1 in the Supporting Information). AdMgA was not considered in the QM/MM MD runs, as this adduct was not stable (vide infra). The last snapshots of the MD runs were employed as starting structures for the QM/MM MD runs.

The QM region was treated at the density functional theory (DFT) level using the Becke−Lee−Yang−Parr (BLYP) exchange-correlation functional.[63,64] CP2K, unlike other DFT packages, implements a dual Gaussian-type/plane wave basis set (GPW);[62] thus, a triple z basis set, an auxiliary basis set with a density cutoff of 280 Ry, and Goedecker−Teter−Hutter[65,66] pseudopotentials were used for all the atoms in the QM region. For the MM part of the system, instead, we used the same FF parameters employed in the classical MD. The valences of the atoms involved in the bonds crossing the QM and the MM boundaries were saturated by adding hydrogen atoms.

Before starting the production runs, the two systems were annealed to relax the starting structures. Then, the temperature was slowly increased up to 298.5 K and the systems were

dx.doi.org/10.1021/jp206475d | J. Phys. Chem. B 2012, 116, 2259−2268

equilibrated for 1 ps. Finally, the two systems were simulated in an NVT ensemble using a Nosè−Hoover chain thermostat for 5 ps, with a time step of 0.48 fs.

2.4. Analysis of RNA Databases. To generalize and validate our findings a detailed comparison of the resulting structural properties of the metal(s) coordination site(s) was done with that of polymerase proteinaceous enzymes and other metal containing ribozymes. This comparison was done using the metals in RNA databases (MeRNA http://merna.lbl.gov/).[40]

2.5. Other Analyses. H-bond, root-mean-square-fluctuation (RMSF), and cluster analysis were done with the *ptraj* module available in AMBER11.[57] In the H-bond analysis, the distance cutoff was set to 3.5 Å and the angle to 120°. The cluster analysis was done with the averagelinkage algorithm, using an RMSD cutoff of 1.5 Å.[67]

The density derived atomic charges[68] for the magnesium ions (Table S3, Supporting Information) have been calculated using CP2K[62] using the same setting of the QM/MM simulations. Visual inspection of the trajectories was carried out with the Visual Molecular Dynamics (VMD) software.[69] This software was used also to prepare all the figures of the ribozyme models.

3. RESULTS AND DISCUSSION

3.1. MD Simulations of the Autoligation Product. Since divalent cations have a very low propensity to diffuse in the time scale currently accessible to classical MD simulations,[70] three different simulations were carried out to determine the positions of the Mg^{2+} ions inside the putative catalytic site by placing a different number of Mg^{2+} and Na^{+} ions in the most negative regions of the electrostatic potential,[70] always obtaining electroneutrality.[17]

The three resulting models were simulated for 30 ns using the AMBER point charges for Mg^{2+}.

In all three simulation conditions, the system shows a similar global RMSD value (calculated on all the RNA heavy atoms) of 5.14 ± 0.35, 4.46 ± 0.44, and 5.13 ± 0.31 Å for the P1, P2, and P3 models, respectively. Moreover, in all simulations, the positions of the experimentally determined ions is not significantly perturbed by the presence of the additional Mg ions (Table S2, Supporting Information). These data are consistent with a recent study reported by Sklenovsky et al.[71] which points out that the ionic concentration has a minor impact on the results of the MD simulations of RNA molecules with respect to other issues such as the choice of the solvation model.

In P1 and P2, a similar RMSF was observed in the vicinity of the putative catalytic site, while, clearly, the addition of more Mg^{2+} ions in P3 induced an overall decrease of the RMSF (Figure S2, Supporting Information). Since the flexibility and RMSD of the putative catalytic site was similar in P1, that conserves only the experimentally solved Mg^{2+} ions, and P2, which contains one Mg^{2+} in the putative active site, and since we know from NAIM experiment that at least one Mg^{2+} is involved in the catalysis, we selected the P2 model for further calculations.

Mg^{2+} was initially located between the phosphate oxygen atoms of A29, C30, and G1 as hypothesized in ref 6, and it maintained these interactions during the entire 30 ns of MD. Three waters completed the Mg^{2+} coordination shell in site A, resulting in an octahedral geometry. The average distances measured between MgA and its coordinating ligands (Table 1) were slightly shorter than those usually reported for a magnesium ion in complex with nucleic acids.[18,41,72] The Mg−O@P and Mg−O@WAT bond lengths were, in fact, of 2.05 ± 0.07 and 1.89 ± 0.05 Å, respectively, as compared with Mg−O@P = 2.12 ± 0.17 Å and Mg−O@WAT = 2.15 ± 0.18 Å obtained from X-ray structures of Mg^{2+} containing enzymes (see section 3.3). However, the position of MgA was consistent with that proposed by NAIM experiments.

Table 1. Average Coordination Bond Lengths (Å) of MgA in P2 during the MD Performed with the Point Charge (PC) and Dummy Cation (DC) Approach for Mg^{2+} [a]

Atom-1	Atom-2	bond lengths (Å), PC	bond lengths (Å), DC
$O^{(R)}$@C30	MgA	1.90 (0.05)	2.32 (0.04)
$O^{(S)}$@A29	MgA	1.88 (0.04)	2.23 (0.07)
$O^{(S)}$@G1	MgA	1.89 (0.05)	2.26 (0.06)
O@Wat1	MgA	2.03 (0.06)	2.37 (0.07)
O@Wat2	MgA	2.05 (0.07)	2.43 (0.07)
O@Wat3	MgA	2.06 (0.07)	2.41 (0.07)

[a]Standard deviations are reported in parentheses. Atom names are reported according to the IUPAC nomenclature.[88]

Interestingly, after the equilibration phase, C47 showed a different position with respect to the crystal structure, breaking its π-stacking interaction with C30 and its H-bond with the $O^{(R)}$@C30. This nucleotide formed, instead, stable H-bonds with A29, C30, and G1 (Table 2 and Figure S3, Supporting Information). The structural rearrangement was most probably due to the MgA ion, which anchored A29 and C30 phosphates, shrinking the putative active site, and subtracting A29 and C30 to the H-bond with NH_2@C47. The reliability of this simulation is confirmed by the fact that C47 conserves its original position over the entire MD simulation of P1, where no magnesium ion is placed between A29 and C30. Instead, C47 underwent a similar rotation in both P2 and P3MD runs.

Table 2. H-Bonds Involving the Nucleotides of the Putative Catalytic Site (A29, C30, G1, and C47) during the Last 20 ns of MD Simulations of P2 Performed with the Point Charge Model[a]

acceptor	donor	mean distance (Å)	% occupancy
N3@G1	NH_2@C47	3.1 (0.18)	67
O2@C47	NH_2@A29	3.0 (0.17)	89
O4′@C47	NH_2@C30	3.0 (0.18)	91

[a]The distance cutoff was set to 3.5 Å and the angle to 120°. Standard deviations are reported in parentheses. The H-bond distances measured during the MD simulation using the dummy cation approach are substantially similar and not reported.

To further relax the geometry of the MgA, we extended our simulation for an additional 20 ns using a dummy cation model.[59] This simulation confirmed that Mg^{2+} was stably bonded in site A, with an octahedral coordination formed by the oxygen atoms of the phosphate groups of G1, A29, and C30 and three waters. The only difference observed with respect to the MD run performed with the point charge model was in the value of the coordination bond lengths, which, using the dummy cation approach, became larger and closer to the typical values of a Mg^{2+} embedded into an enzymatic site.[18,72] In fact, the Mg−O@P and Mg−O@WAT bond lengths were 2.27 ± 0.07 and 2.40 ± 0.07 Å, respectively (Table 1).

In the product state, we can only bind one Mg^{2+}, since the second Mg^{2+} coordinates the PPi moiety of the incoming

dx.doi.org/10.1021/jp206475d | J. Phys. Chem. B 2012, 116, 2259−2268

nucleotide, as observed in DNA and RNA polymerases.[73,74] In the product, the PPi may have been already released from the active site, consistently with the crystal structure of another ligase ribozyme.[5,45,75]

3.2. Force Field Based MD on the Substrate/Ribozyme Adduct. After the preliminary MD simulations performed on the product, we undertook the study of the reactant adducts formed by (U-7)−(A-1) nucleotides, the substrate, and ($G1_{gtp}$)−(A121) nucleotides, the ribozyme (Figure 2).

As for the autoligation product, we initially checked the stability of the adduct considering only MgA. Surprisingly, already after 200 ps of MD, it was clear that MgA by itself did not allow a stable binding of the substrate. In fact, the distance between O3′@A-1 and Pα@$G1_{gtp}$ slowly increased, reaching a value larger than 6 Å, which was incompatible with the catalytic activity.

During the years, a bimetallic mechanism was frequently proposed for DNA and RNA proteinaceous polymerases, as well as other ribozymes with self-cleaving activity.[42,45,75,76] Therefore, according to previous experimental and computational findings on similar systems[18,41,77−79] we placed a second Mg^{2+} ion in the B site, namely, between O3′@A-1 and Pα@$G1_{gtp}$ (MgB), at a distance of 4 Å from MgA (Figure 2). In this case, different initial orientations of the PPi moiety were considered.

During 20 ns of classical MD of AdMgAB using the dummy cation approach, the two ions were stable inside the active site with a MgA−MgB distance of 3.9 ± 0.1 Å.

Also, the substrate maintained the correct geometry to undergo a nucleophilic attack with a mean O3′@A-1···Pα@$G1_{gtp}$ distance of 3.5 ± 0.2 Å. The coordination bond lengths of the two ions (Table 3) and the correct hexa-coordination for both Mg^{2+} were consistent with a bimetallic site. Interestingly, a Na^+ ion lied in the vicinity of the PPi moiety of $G1_{gtp}$, interacting with O1@$G1_{gtp}$ and O6@$G1_{gtp}$ (see Table S2 and Figure S5, Supporting Information). Thus, MgB appeared to be essential for the binding of the substrate, and therefore, we also constructed a model with only MgB.

A 20 ns long MD showed that the substrate remained coordinated and in a favorable position for the nucleophilic attack also in AdMgB. In fact, the O3′@A-1 and Pα@$G1_{gtp}$ distance was 3.46 ± 0.13 Å. In addition, the octahedral coordination geometry was retained, with coordination bond lengths similar to those measured for MgB in AdMgAB (Table 4). Consistent with other polymerases, MgB is placed between the O3′@A-1 and O3 and O9@$G1_{gtp}$ acting as an electrostatic glue for the substrate.[18,41,47] Remarkably, during the simulation of AdMgB, a Na^+ diffused from the bulk to the same site previously occupied by MgA (Figure S4, Supporting Information). Although Na^+ and Mg^{2+} have different net charges, they share a similar hexa-coordinated geometry, suggesting that the A site has a high propensity to host a positive ion.

Although these results may seem in contrast with NAIM experiments, which can detect only MgA, they can be interpreted considering that MgB binds to the PPi moiety and that this may be released, along with the PPi moiety, after the nucleophilic attack, as it occurs in other polymerases.[18,73,80] For these reasons, MgB may be more difficult to detect.

The analysis of the H-bond network of AdMgB and AdMgAB showed that both C30 and C47 were involved in H-bonds with the PPi moiety of $G1_{gtp}$ (Table 5). The H-bond network was substantially similar both in AdMgB and AdMgAB. However, in AdMgAB, the O1@$G1_{gtp}$···NH_2@C47 H-bond had a low occupancy as C47 is slightly shifted toward A-1.

During their experimental studies, Shechner et al.[6] showed that C30U and C47U mutants decrease the enzymatic activity by a factor of 5 and larger than 10^4, respectively. Thus, to confirm the reliability of our findings, we selected the mutation with the largest impact on the catalytic activity and we performed 20 ns of MD simulations for AdMgB-C47U and AdMgAB-C47U. The main difference between C and U was that of impairing the formation of H-bonds with the PPi moiety of $G1_{gtp}$. Notably, Bartel and co-workers hypothesized that C47 stabilizes the PPi moiety of $G1_{gtp}$ via an H-bond interaction.[6] Consistently, our MD simulations of AdMgB-C47U and AdMgAB-C47U did not display any other remarkable difference in the Mg^{2+} coordination sphere with respect to the wild type (WT) ribozyme (Table 3 and Tables S5 and S6, Supporting Information).

Table 3. Average Bond Lengths (Å) of Mg^{2+} Ions and the Coordination Ligands in the Classical MD Runs (CMD) with the Dummy Cation (DC) Approach and the QM/MM MD of the MgAB[a]

coordination sphere of the Mg^{2+} ions		DC CMD	QM/MM MD
Atom-1	Atom-2	distance (Å)	distance (Å)
O3@$G1_{gtp}$	MgB	2.25 (0.05)	2.26 (0.11)
$O^{(S)}$@A29	MgB	2.34 (0.07)	2.26 (0.06)
O9@$G1_{gtp}$	MgB	2.25 (0.05)	2.98 (0.10)
O3′@A-1	MgB	2.33 (0.07)	2.00 (0.05)
$O^{(S)}$@A-1	MgB	2.48 (0.09)	2.17 (0.07)
O@Wat1	MgB	2.36 (0.06)	2.28 (0.09)
O4@$G1_{gtp}$	MgB	2.43 (0.10)	2.67 (0.12)
$O^{(R)}$@C30	MgA	2.27 (0.04)	2.50 (0.06)
$O^{(S)}$@A29	MgA	2.29 (0.06)	2.06 (0.06)
O5@$G1_{gtp}$	MgA	2.26 (0.06)	2.06 (0.05)
O@Wat2	MgA	2.40 (0.06)	2.35 (0.11)
O@Wat3	MgA	2.38 (0.06)	2.47 (0.07)
O@Wat4	MgA	2.49 (0.10)	2.18 (0.10)
MgA	MgB	3.92 (0.10)	4.05 (0.0006)
O3′@A-1	Pα@$G1_{gtp}$	3.54 (0.15)	4.08 (0.10)

[a]Standard deviations are reported in parentheses.

Table 4. Average Bond Lengths (Å) of the Coordination Sphere of MgB in AdMgB Measured along the Classical MD (CMD) with the Dummy Cation (DC) Approach and the QM/MM MD[a]

coordination ligands		CMD DC	QM/MM MD
Atom-1	Atom-2	distance (Å)	distance (Å)
O3@$G1_{gtp}$	MgB	2.24 (0.06)	2.12 (0.06)
$O^{(S)}$@A29	MgB	2.36 (0.12)	1.86 (0.12)
O9@$G1_{gtp}$	MgB	2.23 (0.04)	2.01 (0.06)
O3′@A-1	MgB	2.32 (0.07)	2.46 (0.13)
O4@$G1_{gtp}$	MgB		2.26 (0.06)
$O^{(S)}$@A-1	MgB	2.23 (0.04)	2.36 (0.05)
O@WAT1	MgB	2.48 (0.09)	
O3′@A-1	Pα@$G1_{gtp}$	3.46 (0.13)	3.96 (0.20)

[a]Standard deviations are reported in parentheses.

dx.doi.org/10.1021/jp206475d | J. Phys. Chem. B 2012, 116, 2259−2268

Table 5. H-Bonds Involving C30, C47, and the PPi Moiety of $G1_{gtp}$[a]

AdMgB			
acceptor	donor	mean distance (Å)	% occupancy
O6@$G1_{gtp}$	NH_2@C30	2.83 (0.11)	100
O1@$G1_{gtp}$	NH_2@C47	2.94 (0.13)	99
AdMgAB			
acceptor	donor	mean distance (Å)	% occupation
O6@$G1_{gtp}$	NH_2@C30	2.92 (0.17)	89
O1@$G1_{gtp}$	NH_2@C47	3.18 (0.19)	27

[a]The distance cutoff was set to 3.5 Å and the angle to 120°. Standard deviations are reported in parentheses.

Interestingly, it has been recently pointed out that positively charged residues play an important role in stabilizing the PPi group in DNA polymerases.[43,48,49] In particular, Suo and co-workers,[48,49] on the basis of experimental and bioinformatic studies, evidenced that at least one positively charged residue (Lys or Arg) is conserved in the active site of all DNA polymerases and that this residue usually plays an important role for catalysis, forming a H-bond to PPi and maintaining it anchored to the catalytic site. Moreover, these studies showed that this residue is important but not essential, since the catalytic activity of DNA polymerases remains fairly robust also when the positively charged residue is replaced by a neutral one.[48]

Consistently, in our simulations of WT ribozyme, PPi H-bonds with both C30 and C47, although these residues are neutral. Thus, the C47 rotation observed in both P2 and P3 models (see section 3.1) is necessary to establish the H-bonding interaction with the PPi moiety in all adducts. Furthermore, during the classical MD of the adducts, a Na^+ diffused into the active site and stably interacted with PPi (Table S4, Supporting Information).

The system constituted by C30, C47, and Na^+ strictly resembles the positively charged H-bonding residue observed in a proteinaceous environment. Namely, the two nucleobases are the H-bond donor for the PPi, while the Na^+ provides the positive charge. The reduced catalytic activity displayed by the C47U and the C30U mutants, unable to make H-bonds with the PPi moiety, supports our hypothesis of similarity across ribozyme and enzymatic polymerases.

3.3. QM/MM Calculations. We performed then QM/MM MD to refine the coordination geometry of AdMgAB and AdMgB and to further prove the stability of the magnesium ions inside the putative catalytic site.

These simulations confirmed that AdMgAB was stable (Table 3), although MgB presented a slightly different coordination geometry with respect to the classical MD runs. In fact, during the QM/MM MD simulations, the MgB−O9@$G1_{gtp}$ bond was lost (O9@$G1_{gtp}$−MgB = 2.98 ± 0.1 Å), and the MgB coordinated to O4@$G1_{gtp}$ (2.67 ± 0.12 Å). In this way, MgB maintained a slightly distorted hexa-coordinated geometry (Figure 3). Instead, the coordination geometry of MgA was rather similar to the classical MD, maintaining a hexa-coordinated geometry with three vertexes occupied by waters.

Here, the H-bond between O1@$G1_{gtp}$ and the NH_2@C47 was stronger (2.24 ± 0.24 Å) and, as in the previous MD runs, a Na^+ interacted with O1 and O6 of $G1_{gtp}$ (3.45 ± 0.16 and 3.25 ± 0.08 Å, respectively).

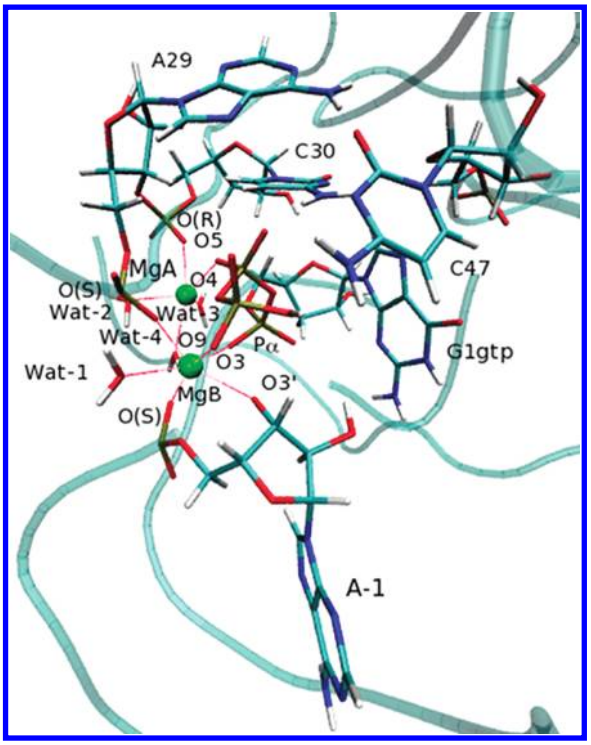

Figure 3. Most representative structure of AdMgAB as obtained from QM/MM MD. MgA is coordinated with O(R)@C30, O(S)@A29, O5@$G1_{gtp}$, O@Wat2, O@Wat3, and O@Wat4; MgB is coordinated with O3@$G1_{gtp}$, O(S)@A29, O9@$G1_{gtp}$, O3′@A-1, O(S)@A-1, O@Wat1, and O4@$G1_{gtp}$. The Na^+ ion coordinated with $G1_{gtp}$ and A71, reported in Figure S5 in the Supporting Information, is here omitted for clarity.

QM/MM MD was also performed for AdMgB. In the initial part of this simulation, the coordination shell of MgB changed with respect to the classical MD trajectory and O@Wat1 was substituted by O4@$G1_{gtp}$. However, also in this case, the adduct was stable during the 5 ps of the QM/MM MD production run with MgB assuming the usual hexa-coordinated geometry (Table 4 and Figure 4).

The distances obtained between the Mg ion and the first shell ligands during the QM/MM MD were in line with those measured in other theoretical studies of bimetallic ribozymes.[42]

The results of these calculations substantially confirmed the correctness of the geometry found during classical MD simulations. The distance between O3′@A-1 and Pα@$G1_{gtp}$ increased to an average value of 4 Å in both AdMgAB and AdMgB.

The average MgA−MgB distance is slightly longer than in the model based on the dummy cation approach, assuming a value slightly larger than 4. Although the two metal ions reaction mechanism of proteinaceous polymerases requires a < 4 Å separation for the ions,[41,44,81] Yang et al.[18] suggested that a MgA−MgB distance of ∼4 Å probably corresponds to a resting state of the enzyme, and that during the reaction a shrinking of this distance may occur. This may lead O3′ closer to Pα, facilitating the nucleophilic attack.

All data from our simulations and from the literature point out that the Mg−O distance is moderately variable and that both the dummy cation and the point charge approaches could reproduce Mg−O coordination bond lengths in line with the experimental values. However, the Mg−O bond lengths obtained via a dummy cation approach were more similar to

dx.doi.org/10.1021/jp206475d | J. Phys. Chem. B 2012, 116, 2259−2268

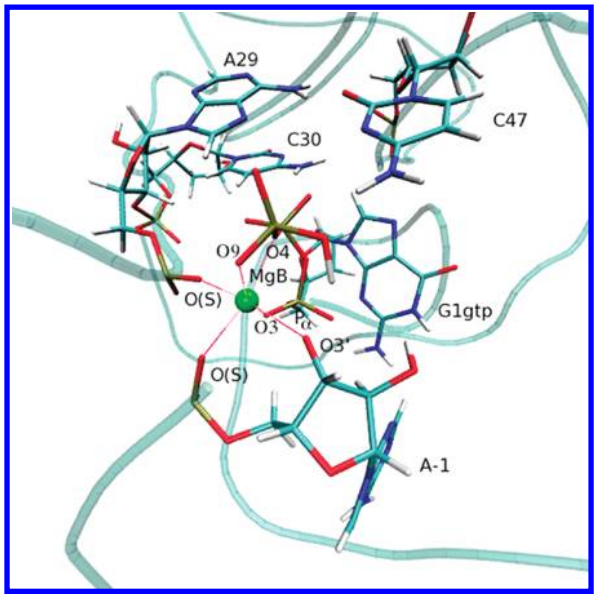

Figure 4. Most representative structure of AdMgB as obtained from QM/MM MD. MgB is coordinated with O3′@A-1, O3@$G1_{gtp}$, O9@$G1_{gtp}$, O4@$G1_{gtp}$, O(S)@A29, and O(S)@A-1.

those measured in our QM/MM MD simulations and in the X-ray structures of other Mg^{2+} containing enzymes (see section 3.3).

3.4. Magnesium Coordination Sphere in Biological Systems. Magnesium ions play a critical role in many aspects of cellular metabolism, stabilizing the structure of nucleic acid and proteins. In addition, they promote catalysis in several enzymes and ribozymes, being particularly relevant in DNA and RNA replication and cleavage.

For example, DNA polymerases, which replicate and repair DNA, critically depend on Mg^{2+} ions. Despite the low sequence similarity across the seven different families, these enzymes are characterized by a common two metal ions mechanism.[18,82] These metals coordinate two highly conserved carboxylate-containing residues (most commonly aspartates) and an additional glutamate or aspartate in the active site[50] (Figure 5A).

RNA polymerases, instead, transcribe DNA into RNA. Despite the significant differences in the sequence and the structures of multisubunit RNA polymerases versus single subunit ones, also these enzymes are characterized by a common catalytic mechanism.[18,82] Furthermore, they present two Mg^{2+} ions, which bind to conserved aspartates in the active site (Figure 5B).[45]

Like proteinaceous DNA and RNA polymerases, the corresponding ribozymes most likely need metal ions in the active site, coordinated in a similar manner. Therefore, it is evident that polymerase/ligase ribozymes may have the same active site structural features and share the same general protein-catalyzed polymerization reaction (Figures 5 and 6).

However, while several experimental and theoretical studies were carried out to unveil and generalize the catalytic mechanisms of proteinaceous enzymes,[41,43,45] to the best of our knowledge, no theoretical study exists to date on RNA ligase ribozymes. The only theoretical studies on the catalytic activity of ribozymes concern, instead, the mechanism of self-cleavage.[25,42]

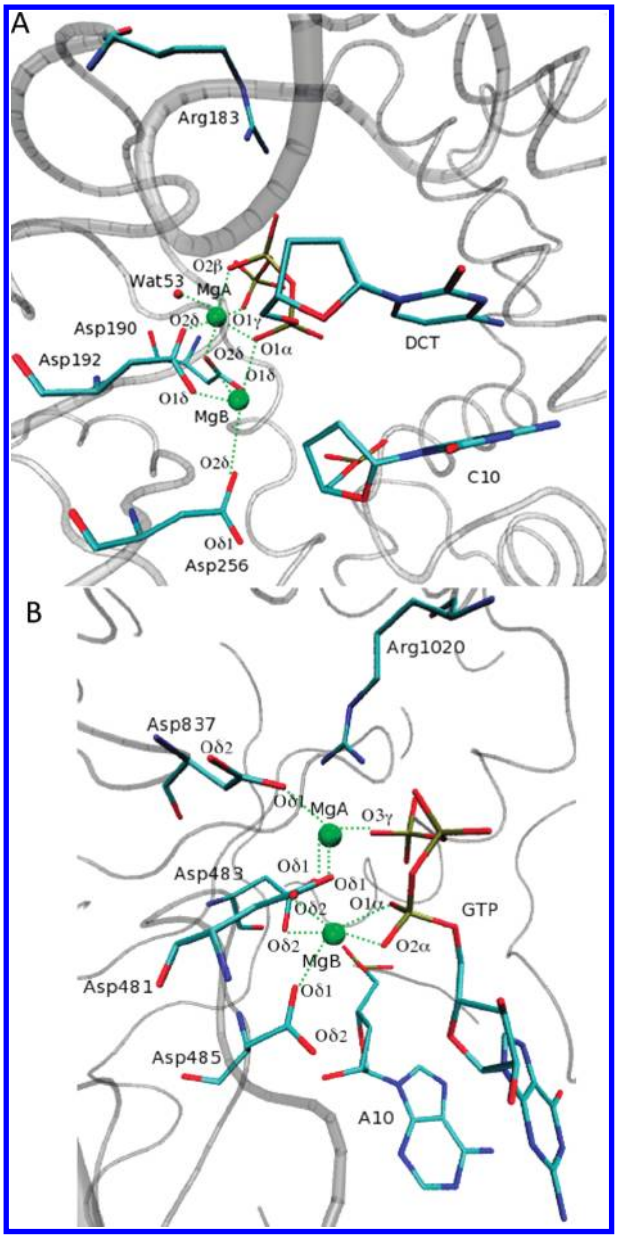

Figure 5. Structural comparison between a representative of a DNA polymerase (A) PBD code 1BYP[74] (MgA is coordinated with O1α@DCT, O2β@DCT, O1γ@DCT, O@WAT53, Oδ2@Asp190, and Oδ2@Asp192; MgB is coordinated with Oδ2@Asp190, Oδ2Asp256, O1α@DCT, Oδ1@Asp192, and Oδ1@Asp190; O3′@C10 is not solved). (B) An RNA polymerase 2E2H[73] (MgA is coordinated with Oδ1@Asp837, O3γ@GTP, Oδ1@Asp483, Oδ1@Asp481; water may complete the coordination shell; MgB is coordinated with O1α@GTP, O2α@GTP, Oδ1@Asp485, Oδ1@483, and Oδ2@Asp483; O3′@C10 is not solved). Hydrogen atoms are not shown for clarity.

To confirm the reliability and generalize the validity of our findings, we compared the structural features obtained from QM/MM MD with that found in the MeRNA database.[40]

We chose the results of the QM/MM MD runs, as an explicit description of the electronic degrees of freedom gives a more reliable description of the Mg^{2+} coordination sphere.

In the PBD database, magnesium ions are invariantly hexa-coordinated with octahedral geometry. An analysis of structures available in the PDB to the 2002[72] indicated that the Mg−O bond length can range between 2.05 and 2.25 Å.

dx.doi.org/10.1021/jp206475d | J. Phys. Chem. B 2012, 116, 2259−2268

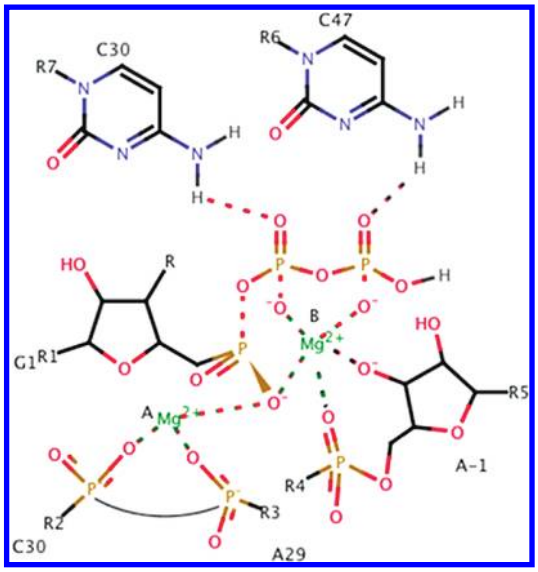

Figure 6. General scheme of the active site for AdMgAB. In AdMgB, the Mg^{2+} in the A site was replaced by a Na^{+} ion.

We also searched in the MeRNA database (http://merna.lbl.gov/),[40] selecting only the X-ray structures with a resolution higher than 2.0 Å. Among these, we selected only the entries where the distance between Mg^{2+} and the oxygen of the phosphates was smaller than 3.0 Å. This resulted in 63 Mg^{2+} binding sites, belonging to 15 different PDBs. This analysis showed a mean Mg−O bond length of 2.12 ± 0.17 Å for the Mg−O@P and of 2.15 ± 0.18 Å for the Mg−O@WAT.

The average coordination bond lengths obtained from QM/MM MD were slightly larger than the crystallographic ones. This was particularly evident for Mg−O@WAT (2.41 ± 0.10 Å), while the average Mg−O@P was in better agreement (2.26 ± 0.08 and 2.18 ± 0.22 Å for AdMgAB and AdMgB, respectively). The slightly larger values of the coordination bond lengths observed in our simulations are consistent with the fact that, different from routine static QM calculations or X-ray structures, our simulations are run in explicit water solvent and are not influenced by crystal packing effects.[83,84] Moreover, the discrepancies between calculated and experimental bond lengths may also depend on the choice of the exchange-correlation functional. In fact, the BLYP[63,64] exchange-correlation functional tends to overestimate coordination bond lengths.[85,31]

Since QM/MM MD simulations are computationally expensive, there are few studies of Mg bound enzymes carried out with this computational approach. These studies report Mg−O@P bond lengths between 2.1 and 2.5 Å, Mg−O3′ in the range of 2.2−2.7 Å, and Mg−O@WAT in the range of 2.1−2.4 Å, which are consistent with our findings.[42,86]

SUMMARY AND CONCLUSIONS

In this paper, we provided a detailed structural characterization of the metal content and of the coordination sphere of the reactant and product states of a class I ligase ribozyme.

By performing a set of classical and QM/MM MD simulations, we identified the number of Mg^{2+} ions inside the catalytic site. Consistently with experimental findings, our simulations revealed that the product state was stable with no or only one metal ion (MgA) coordinated to the backbone of A29 and C30. Instead, the reactant state was stable with two metal ions (with MgA placed in the same binding site of the product and with MgB placed in the vicinity of the PPi moiety of $G1_{gtp}$) or with only MgB. Both AdMgAB and AdMgB simulations led to magnesium coordination geometries with structural features in line with those of proteinaceous DNA and RNA polymerases, whose catalytic activity relies on a two Mg^{2+} ions mechanism.[46,74] Since NAIM experiments suggested that A29 and C30, forming the MgA binding site, are crucial for Mg^{2+} binding and since AdMgA was not stable, it is likely that a two metal ions mechanism may be operative also in ligase ribozymes. As a further proof of this, in the AdMgB model, we saw that after a few ns the MgA binding site was occupied by a Na^{+}, suggesting that this site has a high propensity to host a positively charged ion. However, considering the relatively good tolerance of this ribozyme to low Mg^{2+} concentrations, the fact that both AdMgB and AdMgAB geometries obtained from QM/MM calculations are consistent with literature structural data, along with the possibility reported for the HDV ribozyme to have different active conformations,[87] we cannot completely exclude that a monometallic active species may also be active.

Finally, a comparison between the structural features of proteinaceous nucleic acid polymerase and our findings pointed out strong similarities, supporting the idea that polymerases, ribozymes, and enzymes may share a highly similar catalytic mechanism.

ASSOCIATED CONTENT

Supporting Information

A complete list of QM atoms in the QM/MM calculations; average RMSD values for the 16 conserved Mg^{2+} ions with respect to the crystallographic positions during the MD simulations of the P1, P2, and P3 models, using the single point charge approach; atomic charges used during the classical MD simulation and density derived atomic charges from the QM/MM MD calculations for the catalytic magnesium ions; distances between the Na^{+} ion interacting with the PPi moiety of $G1_{gtp}$ and its coordination shell atoms, measured during the classical MD of AdMgAB; coordination distances for the magnesium ions during the classical MD simulations of the C47U mutants; RMSD during the classical MD simulations for the P1, P2, and P3 models with respect to the crystallographic structure; RMSF values calculated with respect to the X-ray structure for the P1, P2, and P3 models; figure of the C47 conformation in the X-ray structure and in the last snapshot of the MD of the autoligation product; structural comparison between the most representative structures of AdMgAB and AdMgB; figure of the Na^{+} ion interacting with the PPi moiety during the MD simulation. This material is available free of charge via the Internet at http://pubs.acs.org.

AUTHOR INFORMATION

Corresponding Author

*Phone: +39 040 3787 529. Fax: +39 040 3787 528. E-mail: alema@sissa.it.

ACKNOWLEDGMENTS

The authors thank the CINECA and CASPUR supercomputing centers for computational resources.

REFERENCES

(1) Talini, G.; Gallori, E.; Maurel, M. *Res. Microbiol.* **2009**, *160*, 457−465.
(2) Cech, T. R. *Cold Spring Harbor Perspect. Biol.* **2011**, *3*, a006742−a006747.
(3) Scott, W. G. *Curr. Opin. Struct. Biol.* **2007**, *17*, 280−286.
(4) Doudna, J. A.; Lorsch, J. R. *Nat. Struct. Mol. Biol.* **2005**, *12*, 395−402.
(5) Robertson, M. P.; Scott, W. G. *Science* **2007**, *315*, 1549−1553.
(6) Shechner, D. M.; Grant, R. A.; Bagby, S. C.; Koldobskaya, Y.; Piccirilli, J. A.; Bartel, D. P. *Science* **2009**, *326*, 1271−1275.
(7) Cheng, L. K. L.; Unrau, P. J. *Cold Spring Harbor Perspect. Biol.* **2010**, *2*, a002204−a002220.
(8) Wochner, A.; Attwater, J.; Coulson, A.; Holliger, P. *Science* **2011**, *332*, 209−212.
(9) Joyce, G. F. *Science* **2007**, *315*, 1507−1508.
(10) Johnston, W. K.; Unrau, P. J.; Lawrence, M. S.; Glasner, M. E.; Bartel, D. P. *Science* **2001**, *292*, 1319−1325.
(11) Lawrence, M. S.; Bartel, D. P. *RNA* **2005**, *11*, 1173−1180.
(12) Bartel, D. P.; Szostak, J. W. *Science* **1993**, *261*, 1411−1418.
(13) Kuhne, H.; Joyce, G. F. *J. Mol. Evol.* **2003**, *57*, 292−298.
(14) Schmitt, T.; Lehman, N. *Chem. Biol.* **1999**, *6*, 857−869.
(15) Muller, J. *Metallomics* **2010**, *2*, 318−327.
(16) Sigel, R. K. O.; Pyle, A. M. *Chem. Rev.* **2006**, *107*, 97−113.
(17) Frederiksen, J. K.; Piccirilli, J. A. *Methods* **2009**, *49*, 148−166.
(18) Yang, W.; Lee, J. Y.; Nowotny, M. *Mol. Cell* **2006**, *22*, 5−13.
(19) Andreini, C.; Bertini, I.; Cavallaro, G.; Holliday, G.; Thornton, J. *J. Biol. Inorg. Chem.* **2008**, *13*, 1205−1218.
(20) Yang, W. *Q. Rev. Biophys.* **2011**, *44*, 1−93.
(21) Yang, W. *Nat. Struct. Mol. Biol.* **2008**, *15*, 1228−1231.
(22) Bagby, S. C.; Bergman, N. H.; Shechner, D. M.; Yen, C.; Bartel, D. P. *RNA* **2009**, *15*, 2129−2146.
(23) Toor, N.; Keating, K. S.; Taylor, S. D.; Pyle, A. M. *Science* **2008**, *320*, 77−82.
(24) Stahley, M. R.; Strobel, S. A. *Science* **2005**, *309*, 1587−1590.
(25) Lee, T. S.; Giambasu, G. M.; York, D. M. Insights into the Role of Conformational Transitions and Metal Ion Binding in RNA Catalysis from Molecular Simulations. In *Annual Reports in Computational Chemistry*; Ralph, A. W., Ed.; Elsevier: Paris, 2010; Vol. *6*, pp 168−200.
(26) Zimmer, M. *Coord. Chem. Rev.* **2009**, *253*, 817−826.
(27) Spiegel, K.; Magistrato, A. *Org. Biomol. Chem.* **2006**, *4*, 2507−2517.
(28) Bazzicalupi, C.; Bencini, A.; Bonaccini, C.; Giorgi, C.; Gratteri, P.; Moro, S.; Palumbo, M.; Simionato, A.; Sgrignani, J.; Sissi, C.; et al. *Inorg. Chem.* **2008**, *47*, 5473−5484.
(29) Tozzini, V. *Acc. Chem. Res.* **2009**, *43*, 220−230.
(30) Spiegel, K.; Magistrato, A.; Carloni, P.; Reedijk, J.; Klein, M. L. *J. Phys. Chem. B* **2007**, *111*, 11873−11876.
(31) Magistrato, A.; Ruggerone, P.; Spiegel, K.; Carloni, P.; Reedijk, J. *J. Phys. Chem. B* **2005**, *110*, 3604−3613.
(32) Simona, F.; Magistrato, A.; Dal Peraro, M.; Cavalli, A.; Vila, A. J.; Carloni, P. *J. Biol. Chem.* **2009**, *284*, 28164−28171.
(33) Friesner, R. A.; Guallar, V. *Annu. Rev. Phys. Chem.* **2005**, *56*, 389−427.
(34) Lonsdale, R.; Ranaghan, K. E.; Mulholland, A. J. *Chem. Commun.* **2010**, *46*, 2354−2372.
(35) Otyepka, M.; Banas, P.; Magistrato, A.; Carloni, P.; Damborsky, J. *Proteins* **2008**, *70*, 707−717.
(36) Senn, H. M.; Thiel, W. *Angew. Chem., Int. Ed. Engl.* **2009**, *48*, 1198−1229.
(37) Ditzler, M. A.; Otyepka, M.; Sponer, J.; Walter, N. G. *Acc. Chem. Res.* **2009**, *43*, 40−47.
(38) Colombo, M. C.; Guidoni, L.; Laio, A.; Magistrato, A.; Maurer, P.; Piana, S.; Rohrig, U.; Spiegel, K.; Sulpizi, M.; VandeVondele, J.; et al. *Chimia* **2002**, *56*, 13−19.
(39) Banáš, P.; Jurecka, P.; Walter, N. G.; Sponer, J.; Otyepka, M. *Methods* **2009**, *49*, 202−216.
(40) Stefan, L. R.; Zhang, R.; Levitan, A. G.; Hendrix, D. K.; Brenner, S. E.; Holbrook, S. R. *Nucleic Acids Res.* **2006**, *34*, 131−134.
(41) Rungrotmongkol, T.; Mulholland, A. J.; Hannongbua, S. *J. Mol. Graphics Modell.* **2007**, *26*, 1−13.
(42) Boero, M.; Tateno, M.; Terakura, K.; Oshiyama, A. *J. Chem. Theory Comput.* **2005**, *1*, 925−934.
(43) Cisneros, G. A.; Perera, L.; Garcia-Diaz, M.; Bebenek, K.; Kunkel, T. A.; Pedersen, L. G. *DNA Repair* **2008**, *7*, 1824−1834.
(44) Chaudret, R.; Piquemal, J.-P.; Andres Cisneros, G. *Phys. Chem. Chem. Phys.* **2011**, *13*, 11239−11247.
(45) Carvalho, A. T. P.; Fernandes, P. A.; Ramos, M. J. *J. Chem. Theory Comput.* **2011**, *7*, 1177−1188.
(46) Yang, L.; Arora, K.; Beard, W. A.; Wilson, S. H.; Schlick, T. *J. Am. Chem. Soc.* **2004**, *126*, 8441−8453.
(47) Castro, C.; Smidansky, E. D.; Arnold, J. J.; Maksimchuk, K. R.; Moustafa, I.; Uchida, A.; Gotte, M.; Konigsberg, W.; Cameron, C. E. *Nat. Struct. Mol. Biol.* **2009**, *16*, 212−218.
(48) Fowler, J. D.; Brown, J. A.; Kvaratskhelia, M.; Suo, Z. *J. Mol. Biol.* **2009**, *390*, 368−379.
(49) Brown, J. A.; Pack, L. R.; Sherrer, S. M.; Kshetry, A. K.; Newmister, S. A.; Fowler, J. D.; Taylor, J.-S.; Suo, Z. *J. Mol. Biol.* **2010**, *403*, 505−515.
(50) Steitz, T. A.; Steitz, J. A. *Proc. Natl. Acad. Sci. U.S.A.* **1993**, *90*, 6498−6502.
(51) Wang, J.; Cieplak, P.; Kollman, P. *J. Comput. Chem.* **2000**, *21*, 1049−1074.
(52) Perez, A.; Marchan, I.; Svozil, D.; Sponer, J.; Cheatham, T. E.; Laughton, C. A.; Orozco, M. *Biophys. J.* **2007**, *92*, 3817−3829.
(53) Aaqvist, J. *J. Chem. Phys.* **1990**, *94*, 8021−8024.
(54) Jorgensen, W. L.; Chandrasekhar, J.; Madura, J. D.; Impey, R. W.; Klein, L. M. *J. Chem. Phys.* **1983**, *79*, 926−935.
(55) Homeyer, N.; Essigke, T.; Meiselbach, H.; Ullmann, G.; Sticht, H. *J. Mol. Model.* **2007**, *13*, 431−444.
(56) Frisch, M. J.; Trucks, G. W.; Schlegel, H. B.; Scuseria, G. E.; Robb, M. A.; Cheeseman, J. R.; Montgomery, J. A.; Vreven, T.; Kudin, K. N.; Burant, J. C.;et al. *Gaussian 03*, revision C.02; Gaussian, Inc.: Wallingford, CT, 2003.
(57) Case, D. A.; T. A. D.; Cheatham, T. E., III; Simmerling, C. L.; Wang, J.; Duke, R. E.; Luo, R. C. W.; Zhang, W.; Merz, K. M.; Roberts, B.; et al. *AMBER11*; University of California: San Francisco, CA, 2010.
(58) Phillips, J. C.; Braun, R.; Wang, W.; Gumbart, J.; Tajkhorshid, E.; Villa, E.; Chipot, C.; Skeel, R. D.; Kale, L.; Schulten, K. *J. Comput. Chem.* **2005**, *26*, 1781−1802.
(59) Oelschlaeger, P.; Klahn, M.; Beard, W. A.; Wilson, S. H.; Warshel, A. *J. Mol. Biol.* **2007**, *366*, 687−701.
(60) Aaqvist, J.; Warshel, A. *J. Am. Chem. Soc.* **1990**, *112*, 2860−2868.
(61) Laino, T.; Mohamed, F.; Laio, A.; Parrinello, M. *J. Chem. Theory Comput.* **2005**, *1*, 1176−1184.
(62) VandeVondele, J.; Krack, M.; Mohamed, F.; Parrinello, M.; Chassaing, T.; Hutter, J. *Comput. Phys. Commun.* **2005**, *167*, 103−128.
(63) Becke, A. D. *Phys. Rev. A* **1988**, *38*, 3098.
(64) Lee, C.; Yang, W.; Parr, R. G. *Phys. Rev. B* **1988**, *37*, 785.
(65) Goedecker, S.; Teter, M.; Hutter, J. *Phys. Rev. B* **1996**, *54*, 1703.
(66) Hartwigsen, C.; Goedecker, S.; Hutter, J. *Phys. Rev. B* **1998**, *58*, 3641.
(67) Shao, J.; Tanner, S. W.; Thompson, N.; Cheatham, T. E. *J. Chem. Theory Comput.* **2007**, *3*, 2312−2334.
(68) Blochl, P. *J. Chem. Phys.* **1995**, *103*, 7422−7428.
(69) Humphrey, W.; Dalke, A.; Schulten, K. *J. Mol. Graphics* **1996**, *14*, 33−38.
(70) Hashem, Y.; Auffinger, P. *Methods* **2009**, *47*, 187−197.
(71) Sklenovsky, P.; Florova, P.; Banas, P.; Reblova, K.; Lankas, F.; Otyepka, M.; Sponer, J. *J. Chem. Theory Comput.* **2011**, *7*, 2963−2980.
(72) Maguire, M. E.; Cowan, J. A. *Biometals* **2002**, *15*, 203−210.
(73) Yin, Y. W.; Steitz, T. A. *Cell* **2004**, *116*, 393−404.
(74) Sawaya, M. R.; Prasad, R.; Wilson, S. H.; Kraut, J.; Pelletier, H. *Biochemistry* **1997**, *36*, 11205−11215.
(75) Yang, L. J.; Arora, K.; Beard, W. A.; Wilson, S. H.; Schlick, T. *J. Am. Chem. Soc.* **2004**, *126*, 8441−8453.

(76) Cisneros, G. A.; Perera, L.; Schaaper, R. M.; Pedersen, L. C.; London, R. E.; Pedersen, L. G.; Darden, T. A. *J. Am. Chem. Soc.* **2009**, *131*, 1550−1556.
(77) Wang, Y.; Schlick, T. *J. Am. Chem. Soc.* **2008**, *130*, 13240−13250.
(78) Huang, H.; Chopra, R.; Verdine, G. L.; Harrison, S. C. *Science* **1998**, *282*, 1669−1675.
(79) Rechkoblit, O.; Malinina, L.; Cheng, Y.; Kuryavyi, V.; Broyde, S.; Geacintov, N. E.; Patel, D. J. *PLoS Biol.* **2006**, *4*, e11.
(80) Vaisman, A.; Ling, H.; Woodgate, R.; Yang, W. *EMBO J.* **2005**, *24*, 2957−2967.
(81) Gleghorn, M. L.; Davydova, E. K.; Basu, R.; Rothman-Denes, L. B.; Murakami, K. S. *Proc. Natl. Acad. Sci. U.S.A.* **2011**, *108*, 3566−3571.
(82) Steitz, T. A. *Nature* **1998**, *391*, 231−232.
(83) Petrov, A. S.; Bowman, J. C.; Harvey, S. C.; Williams, L. D. *RNA* **2010**, *17*, 291−297.
(84) Magistrato, A.; DeGrado, W. F.; Laio, A.; Rothlisberger, U.; VandeVondele, J.; Klein, M. L. *J. Phys. Chem. B* **2003**, *107*, 4182−4188.
(85) VandeVondele, J.; Magistrato, A.; Rothlisberger, U. *Inorg. Chem.* **2001**, *40*, 5780−5786.
(86) Ho, M.-H.; De Vivo, M.; Dal Peraro, M.; Klein, M. L. *J. Am. Chem. Soc.* **2010**, *132*, 13702−13712.
(87) Nakano, S.; Proctor, D. J.; Bevilacqua, P. C. *Biochemistry* **2001**, *40*, 12022−12038.
(88) IUPAC-IUB Joint Commission on Biochemical Nomenclature (JCBN). *Eur. J. Biochem.* **1983**, *131*, 9−15.